Enhanced surface sensitivity in microring resonator biosensor based on subwavelength grating waveguides

Hai Yan[a], Lijun Huang[a,b], Xiaochuan Xu[c], Naimei Tang[c], Swapnajit Chakravarty[c], Ray T. Chen[a, c,*]
[a]Department of Electrical and Computer Engineering, The University of Texas at Austin, Austin, TX 78758, USA;
[b]State Key Laboratory of Information Photonics and Optical Communications, School of Information and Communication Engineering, Beijing University of Posts and Telecommunications, Beijing 100876, China
[c]Omega Optics Inc., 8500 Shoal Creek Blvd., Austin, TX, 78759, USA
[*]raychen@uts.cc.utexas.edu

ABSTRACT

Microring resonators on silicon-on-insulator substrate have been demonstrated to be promising in sensing applications. We study a microring resonator biosensor based on a novel subwavelength grating (SWG) waveguide structure, which consists of periodic silicon pillars in the propagation direction with a subwavelength period. In this structure, effective sensing region includes not only the top and side of the waveguide, but also the space in between the silicon pillars which is on the path of the propagation mode. This leads to greatly increased bulk refractive index sensitivity as well as extended surface sensing region with constantly high surface sensitivity.

Keywords: subwavelength grating waveguides, microring resonators, integrated optical biosensors, surface sensing, integrated photonics

1. INTRODUCTION

Integrated photonic devices attract increasing attention as a candidate for high-sensitivity on-chip biosensors. The devices take advantage of the interaction between strongly localized light and the biological targets to be detected, enabling label-free detection on a micro/nano-scale region[1–3]. Various devices, including microring resonators[4,5], silicon nanowires[6], nanoporous silicon waveguides[7], photonic crystal (PC) microcavities[8–10], have been proposed and demonstrated. Most of the proposed structures are based on the interaction between the evanescent wave and the biomolecules that are absorbed or immobilized on the sensor surface. For example, microring resonators built on silicon-on-insulator (SOI) substrate can detect biomolecule layers immobilized on the surface of the microring through the induced resonance shift in the transmission spectrum[4]. Extensive efforts have been made on this type of sensors focusing on increasing the sensitivity and lowering the detection limit. However, this type of evanescent wave sensing mechanism faces limitation in surface sensing: the sensitivity drops inevitably with increasing thickness of the surface layer accumulated on the sensor surface. In real applications, this layer includes necessary oxide and chemical layers generated by surface treatment, probe proteins, target proteins and any other reagents that are used to enhance the signal. These can amount to a total layer thickness ranging from several nanometers to a few tens of nanometers, within which the sensitivity of the evanescent wave could drop considerably before it reaches the final target to be detected.

Recently, novel subwavelength grating (SWG) based waveguides and photonic devices were proposed and demonstrated[11–14]. The SWG waveguide consists of periodic silicon pillars in the propagation direction with a period much smaller than the operating wavelength. Within such a structure, the wave propagates in a similar way to conventional strip waveguides, but the interaction region between light and the cladding materials is greatly extended compared to the aforementioned evanescent wave based biosensors. Therefore, SWG structure shows great promise in integrated optical biosensors. In [14], microring resonators based on SWG waveguides were first demonstrated with bulk sensitivity (the ratio of resonance shift to the change of surrounding refractive index) greater than 400 nm/RIU, which is several times higher than conventional microring resonators based on strip waveguides[4]. However, the enhanced surface

Frontiers in Biological Detection: From Nanosensors to Systems IX, edited by
Amos Danielli, Benjamin L. Miller, Sharon M. Weiss, Proc. of SPIE Vol. 10081, 100810G
 · doi: 10.1117/12.2250408

sensing capability in SWG waveguide, which is a unique advantage in this structure, has never been revealed and carefully studied.

In this paper, we analyzed and demonstrated enhanced surface sensing capability in microring resonator biosensor based on SWG waveguide structures. In the SWG waveguides, effective sensing region includes not only the top and side of the waveguide, where evanescent wave exists, but also the space between silicon pillars on the light propagation path. This leads to greatly increased sensitivity as well as a unique property of thickness-independent surface sensitivity in comparison to conventional microring resonator biosensors. The surface sensitivity (the ratio of resonance shift to the change of surface layer thickness) remains constantly high in SWG microring resonator even when surface layer thickness grows. Simulation shows that the surface sensitivity remains around 1.0 nm/nm in the first 25-nm thick layer upon the surface in the studied case. In the experimental demonstration, microring resonator biosensors based on both SWG waveguides and conventional strip waveguide were fabricated and compared side by side in a biosensing experiment. A comparison between the two types of sensors in the biosensing test verified the superior surface sensing capability in the sensors constructed by SWG waveguides.

2. SIMULATION AND ANALYSIS

The structure of the SWG microring resonator is shown in Fig. 1. It is constructed by replacing the strip waveguides in a regular microring resonator with SWG waveguides. The silicon SWG microring resonator sits on top of the buried oxide layer and is covered by sensing medium (water or other biological buffers). In this paper, the SWG in the microring resonator uses trapezoidal pillars to minimize bending loss, thus to achieve better quality factors[15]. The SWG in the bus waveguide still uses regular rectangular pillars.

The structural parameters of the SWG microring are also marked in Fig. 1. The radius of the microring R is set to 10 μm to achieve high intrinsic quality factor and compact size at the same time. The grating period of the SWG is Λ = 200 nm, which satisfies the condition $\lambda / \Lambda > 2n_{eff}$ (λ = 1550 nm), so the waveguide operates in the subwavelength regime and behaves like a conventional waveguide. Duty cycle of the grating (ratio of silicon pillar length l to grating period Λ) η and waveguide width w are determined through simulation to achieve large optical field overlap with the sensing medium. η = 0.65 and w = 450 nm are chosen, resulting in the calculated overlapping factor σ = 0.4 (defined as the ratio of the electric field inside the low refractive index medium region). So the length of the rectangular pillar is $l = \eta\Lambda$ = 130 nm. The gap between microring and the bus waveguide is d = 50 nm, which is determined by a parameter scanning in fabrication to achieve high quality factor and extinction ratio. For the trapezoidal pillars in the SWG microring, the grating period is the same as the straight waveguide. Widths of the top base (a) and bottom base (b) are determined by minimizing the bending loss in the microring using 3D finite difference time domain (FDTD) simulation[15]. The optimized a and b are 100 nm and 150 nm, respectively. The height of the silicon layer is h = 220 nm.

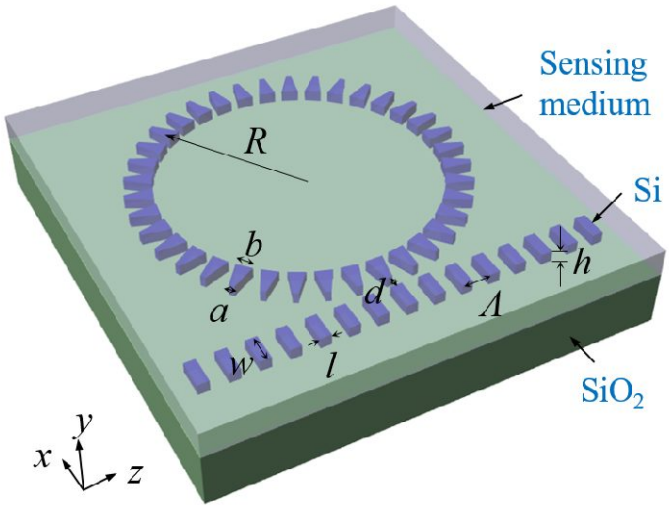

Fig. 1. Schematic of the studied SWG microring resonator biosensor.

The mode profile simulated with the above parameters is shown in Fig.2. Figure 2(a) shows the field between pillars cutting close to the edge of the pillar (*yz* plane at *x* close to edge of the pillar); Figure 2(b) is the electric field distribution at the middle height of the pillar (*xz* plane at *y=h/2*); Figure 2(c) shows the electric field between pillars (*xy* plane at *z*=constant). From the mode profile, it can be seen that in contrast to the evanescent field on the top surface and sidewalls of the waveguide, there is significantly stronger mode field existing on the light propagation path between silicon pillars. In Fig. 2(a), it is especially clear that the field is strongly confined between silicon pillars. This gives SWG based microring biosensors extended surface sensing region on the propagation path and thus unique advantage in surface sensing over conventional microrings.

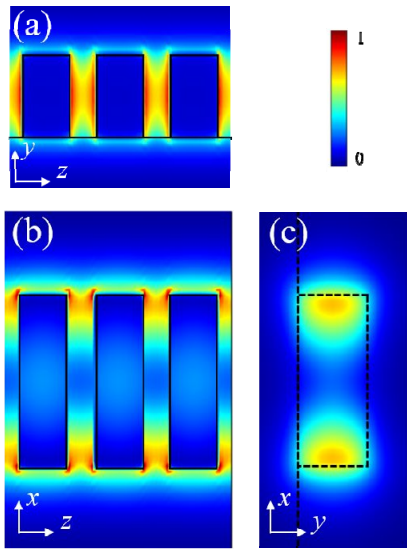

Fig. 2. Electric field intensity distribution at different cross sections: (a) *yz* plane at *x* close to edge of the pillar; (b) *xz* plane at *y=h/2*; (c) *xy* plane at *z*=constant.

In a microring resonator biosensor, the resonance wavelength shifts as the biomolecules interact with the optical field on the surface of the microring. Specific biomolecules can be detected by immobilizing them on the surface through specific biochemical interactions. The surface layer can add up to a thickness from a few nanometers to several tens of nanometers[14,16–19], including silicon dioxide layer (~5nm), chemical layer (several nanometers, generated after surface treatment with (3-Aminopropyl) triethoxysilane (APTES), glutaraldehyde, etc.) and protein layers (antibodies, antigens, etc., several nanometers per layer). Therefore, surface sensitivity is an important figure of merit. In resonance based sensing method, surface sensitivity S_s can be defined as the resonance wavelength shift in according to the change of surface layer thickness[20]:

$$S_s = \frac{\Delta\lambda}{\Delta t} = \frac{\lambda}{n_g}\left(\frac{\partial n_{eff}}{\partial t}\right) \tag{1}$$

where n_g is group index and t is the thickness of surface layer. We assume the sensing medium is water (n = 1.32) and the surface layer has uniform thickness across the surface with uniform refractive index of n = 1.48.[12,14,21] Then the susceptibility $\partial n_{eff} / \partial t$ in the periodic SWG structure is calculated from effective index (n_{eff}) simulation using the 3D PWE solver. The SWG structure has the same parameters as presented above. $\partial n_{eff} / \partial t$ in conventional strip waveguide (w = 500 nm, h = 220 nm, used to form regular microring resonator) is calculated in an eigenmode solver using finite element method (FEM). The simulation results are shown in Fig. 3. The $\partial n_{eff} / \partial t$ in SWG waveguide is 4-6 times larger than that in a regular strip waveguide due to large mode overlapping factor ($\sigma \sim 0.4$). Furthermore, the value remains constantly high in SWG structure for the first 25nm of the surface layer, while in regular strip waveguide, $\partial n_{eff} / \partial t$ drop monotonically with the accumulation of surface layer. This simulation result coincides with the above mode profile analysis that the field confined between silicon pillars extends the surface sensing region and the surface sensitivity becomes insensitive to surface layer thickness. It shows that SWG structure has superior surface sensing capability over

evanescent wave based sensors like conventional microring resonator, in terms of both absolute surface sensitivity S_s and the ability to maintain high surface sensitivity when the thickness of surface layer grows.

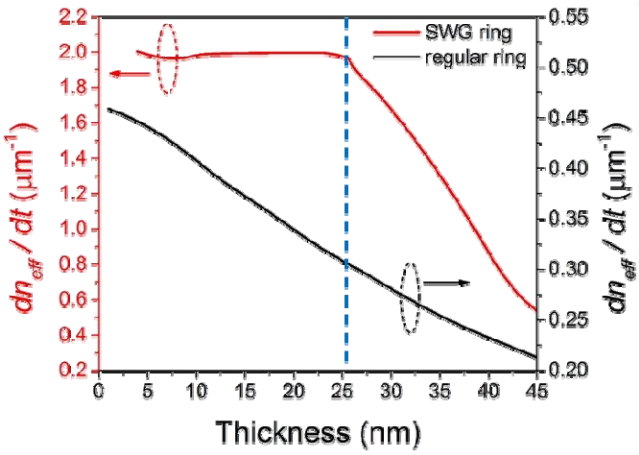

Fig. 3. Comparing dn_{eff}/dt as the thickness of surface layer grows in SWG microring and conventional microring.

3. EXPERIMENTAL RESULTS

Devices were fabricated on a silicon-on-insulator (SOI) wafer with 220 nm thick top silicon layer. The wafer was first patterned by e-beam lithography with ZEP 520A resist (Zeon Chemicals). Then a single reactive ion etching (RIE) process using HBr and Cl_2 is used to transfer the pattern to silicon. Resist was then removed.

After fabrication, the bulk refractive index sensitivity of the SWG microring biosensor was characterized. The resonance peak wavelength was monitored during the experiment. Thus, the bulk sensitivity can be estimated by a linear fit on the resonance shift versus refractive index change plot, as shown in Fig. 4. The fit curve shows a bulk sensitivity of S_b = 440.5 ± 4.2 nm/RIU, which is a typical value for SWG microring resonators[14], and is about 4 times of that of a conventional microring resonator[4]. Scanning electron microscope (SEM) images of the fabricated SWG microring resonator are shown in the inset of Fig. 4 with the coupling region enlarged to show the trapezoidal pillars in the microring and the rectangular pillars in the bus waveguide. A transmission spectrum of the SWG microring is also shown in the inset of Fig. 4, from which the free spectral range is measured to be 12.5 nm, corresponding to group index $n_g = \lambda^2 / (2\pi R \cdot FSR) = 3.0$. The estimated quality factor ($Q \sim \lambda / \delta\lambda$) is as high as 9100 due to the use of trapezoidal pillars in the SWG microring. Considering the high quality factor, the detection limit of the sensor is $DL = \lambda / (Q \cdot S_b) = 3.9 \times 10^{-4}$ RIU. The trapezoidal shape induces pre-distorted refractive index profile to reduce mode mismatch and radiation loss in the SWG bend. It is also worth noting that the absorption loss in water contributes to the total loss in the SWG microring. Moving to a shorter wavelength such as 1310 nm for operation and adjust the design slightly to compensate for the wavelength change would potentially further improve the quality factor. The device would suffer about an order of magnitude less absorption loss[20].

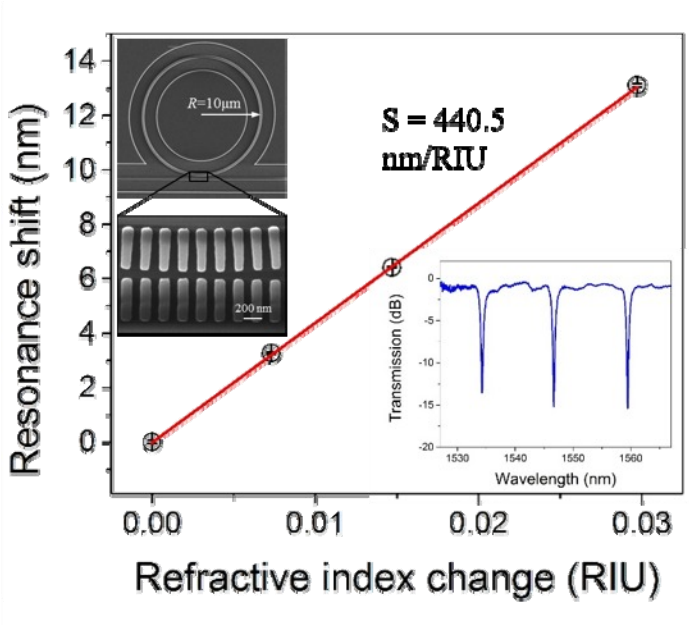

Fig. 4. Resonance shift with respect to refractive index change. Linear fit shows a bulk sensitivity of 440.5 nm/RIU. Insets show scanning electron microscope (SEM) image of the SWG microring resonator with its coupling region enlarged and transmission spectrum of the fabricated SWG microring resonator.

To demonstrate the enhanced surface sensitivity in SWG microring resonators, both SWG microring resonator and regular microring resonator were fabricated on the same chip and compared in a surface sensing test. The regular microring resonator has the same radius of 10 μm and the waveguide is 450 nm wide by 220 nm high. Before the test, the chip was first silanized by 2% (v/v) APTES in toluene. Then the chip was further treated with 2.5% (v/v) glutaraldehyde in phosphate buffer saline (PBS) to provide aldehyde group linker that is able to immobilize protein covalently[16,19]. Next, anti-streptavidin antibody (50 μg/mL, from Abcam), bovine serum albumin (BSA, 1 mg/mL), streptavidin (100 μg/mL, from Sigma-Aldrich), and biotinylated BSA (1 mg/mL, from Thermo Fisher Scientific) were flowed in sequence into the microfluidic channel containing both microring sensors. Anti-streptavidin antibody was immobilized on the sensor surface as probe protein. BSA was used as blocking buffer to block any vacant sites. Streptavidin binds to probe protein and later capture biotinylated BSA through biochemical interactions. Before switching reagent at each of the above steps, PBS buffer was flowed to remove any unbound biomolecules. Resonance wavelengths of both the SWG and conventional microring resonator were recorded and resonance shifts were compared.

The experimental results are shown in Fig. 5. The resonance shifts for both microring biosensors are shown in Fig. 5(a). Resonance shift in SWG microring are several times larger than that in regular microring as expected, because of the much larger overlapping factors in SWG microring. It can also be seen in this figure that with more and more layers built on the surface, the resonance shift difference between the two microrings also becomes larger. To explicitly show this difference, surface sensitivity with respect to the thickness of surface layer is compared in both rings as shown in Fig. 5(b). The thickness of the surface layers is estimated by combining the simulated surface sensitivity and the experimental resonance shift in SWG microring. According to Equation (1) and the simulation in Fig.3, the surface sensitivity of the SWG ring is $S_s \approx 1.0 nm/nm$ (λ = 1550 nm, n_g = 3.0, assume n = 1.48 across all surface layer[12,14,21]) for the first 25 nm thick of surface layer. Therefore, the surface layer thickness can be estimated ($\Delta t = \Delta\lambda / S_s$). The surface sensitivity of the regular microring can then be calculated by the first part of Equation (1) ($S_s = \Delta\lambda / \Delta t$). Figure 5(b) shows that the sensitivity of the microring resonator drops monotonically compared to that of the SWG ring as thickness of accumulated biomolecules grows continuously. It is worth noting that both devices were tested side by side in the same microfluidic channel, the surface layer thickness can be taken as the same, thus the resonance shift at each thickness can be compared. The estimated thickness in the *x*-axis of Fig. 5(b) also takes into account the initial thickness of silicon dioxide (~5 nm) and APTES (~5nm).

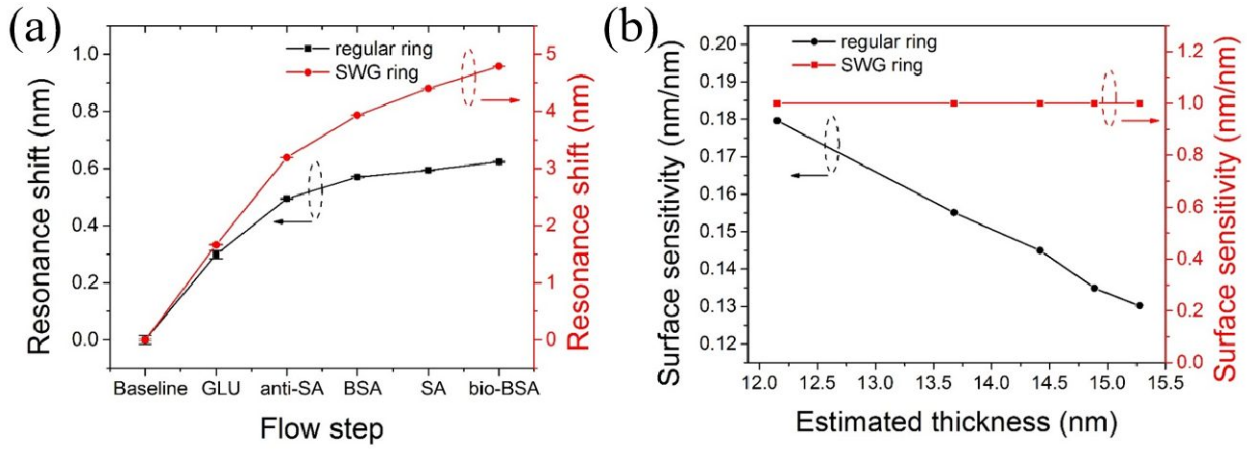

Fig. 5. (a) Resonance shift in both SWG microring and regular microring; GLU: glutaraldehyde (b) Surface sensitivity with respect to estimated thickness in both SWG microring and regular microring.

4. CONCLUSION

In conclusion, we have shown that microring resonator biosensors based on SWG waveguides possess unique property of thickness-independent surface sensitivity and enhanced sensitivity compared to conventional microring resonators. Numerical simulation reveals that due to periodic pillar structure in the propagation direction, the effective sensing region includes not only top surface and sidewall of the waveguide, but also the space on the propagation path between the periodic pillars. It is the strong optical field between the periodic pillars that leads to significantly enhanced interaction with the sensing medium. Biosensing experiment on both SWG microring and conventional microring demonstrated the superior surface sensing capability of the SWG waveguide.

ACKNOWLEDGMENT

The authors would like to acknowledge the support by Department of Energy (DOE) (Contract #: DE SC-0013178) and National Cancer Institute/ National Institutes of Health (NCI/NIH) (Contract #: HHSN261201500039C). L. Huang would like to acknowledge the support by National Natural Science Foundation of China (No. 61372038), Fund of State Key Laboratory of Information Photonics and Optical Communications (Beijing University of Posts and Telecommunications)-IPOC2015ZC02, China and Postgraduate Innovation Fund of SICE, BUPT, 2015. L. Huang also acknowledges the China Scholarship Council (CSC) (NO. 201506470010) for scholarship support.

REFERENCES

[1] Estevez, M. C. C., Alvarez, M.., Lechuga, L. M. M., "Integrated optical devices for lab-on-a-chip biosensing applications," Laser Photon. Rev. **6**(4), 463–487 (2012).

[2] Passaro, V., Tullio, C., Troia, B., Notte, M., Giannoccaro, G.., Leonardis, F., "Recent Advances in Integrated Photonic Sensors," Sensors **12**(12), 15558–15598 (2012).

[3] Vollmer, F., Yang, L.., Fainman, S., "Label-free detection with high-Q microcavities: A review of biosensing mechanisms for integrated devices," Nanophotonics **1**(3–4), 267–291 (2012).

[4] Iqbal, M., Gleeson, M. A., Spaugh, B., Tybor, F., Gunn, W. G., Hochberg, M., Baehr-Jones, T., Bailey, R. C.., Gunn, L. C., "Label-Free Biosensor Arrays Based on Silicon Ring Resonators and High-Speed Optical Scanning Instrumentation," IEEE J. Sel. Top. Quantum Electron. **16**(3), 654–661 (2010).

[5] McClellan, M. S., Domier, L. L.., Bailey, R. C., "Label-free virus detection using silicon photonic microring resonators," Biosens. Bioelectron. **31**(1), 388–392 (2012).

[6] Janz, S., Xu, D.-X., Vachon, M., Sabourin, N., Cheben, P., McIntosh, H., Ding, H., Wang, S., Schmid, J. H., et

al., “Photonic wire biosensor microarray chip and instrumentation with application to serotyping of Escherichia coliisolates.,” Opt. Express **21**(4), 4623–4637 (2013).
[7] Wei, X., Mares, J. W., Gao, Y., Li, D.., Weiss, S. M., “Biomolecule kinetics measurements in flow cell integrated porous silicon waveguides,” Biomed. Opt. Express **3**(9), 1993 (2012).
[8] Yan, H., Zou, Y., Chakravarty, S., Yang, C.-J., Wang, Z., Tang, N., Fan, D.., Chen, R. T., “Silicon on-chip bandpass filters for the multiplexing of high sensitivity photonic crystal microcavity biosensors,” Appl. Phys. Lett. **106**(12), 121103 (2015).
[9] Liang, F., Clarke, N., Patel, P., Loncar, M.., Quan, Q., “Scalable photonic crystal chips for high sensitivity protein detection.,” Opt. Express **21**(26), 32306–32312 (2013).
[10] Lai, W.-C., Chakravarty, S., Zou, Y., Guo, Y.., Chen, R. T., “Slow light enhanced sensitivity of resonance modes in photonic crystal biosensors,” Appl. Phys. Lett. **102**(4), 41111 (2013).
[11] Bock, P. J., Cheben, P., Schmid, J. H., Lapointe, J., Delâge, A., Janz, S., Aers, G. C., Xu, D.-X., Densmore, A., et al., “Subwavelength grating periodic structures in silicon-on-insulator: a new type of microphotonic waveguide,” Opt. Express **18**(19), 20251, Optical Society of America (2010).
[12] Gonzalo Wangüemert-Pérez, J., Cheben, P., Ortega-Moñux, A., Alonso-Ramos, C., Pérez-Galacho, D., Halir, R., Molina-Fernández, I., Xu, D.-X.., Schmid, J. H., “Evanescent field waveguide sensing with subwavelength grating structures in silicon-on-insulator,” Opt. Lett. **39**(15), 4442 (2014).
[13] Donzella, V., Sherwali, A., Flueckiger, J., Grist, S. M., Fard, S. T.., Chrostowski, L., “Design and fabrication of SOI micro-ring resonators based on sub-wavelength grating waveguides,” Opt. Express **23**(4), 4791 (2015).
[14] Flueckiger, J., Schmidt, S., Donzella, V., Sherwali, A., Ratner, D. M., Chrostowski, L.., Cheung, K. C., “Sub-wavelength grating for enhanced ring resonator biosensor,” Opt. Express **24**(14), 15672, Optical Society of America (2016).
[15] Wang, Z., Xu, X., Fan, D., Wang, Y.., Chen, R. T., “High quality factor subwavelength grating waveguide micro-ring resonator based on trapezoidal silicon pillars,” Opt. Lett. **41**(14), 3375, Optical Society of America (2016).
[16] Subramanian, A., Kennel, S. J., Oden, P. I., Jacobson, K. B., Woodward, J.., Doktycz, M. J., “Comparison of techniques for enzyme immobilization on silicon supports,” Enzyme Microb. Technol. **24**(1–2), 26–34 (1999).
[17] Howarter, J. A.., Youngblood, J. P., “Optimization of Silica Silanization by 3-Aminopropyltriethoxysilane,” Langmuir **22**(26), 11142–11147, American Chemical Society (2006).
[18] Grist, S. M., Schmidt, S. a., Flueckiger, J., Donzella, V., Shi, W., Talebi Fard, S., Kirk, J. T., Ratner, D. M., Cheung, K. C., et al., “Silicon photonic micro-disk resonators for label-free biosensing,” Opt. Express **21**(7), 7994 (2013).
[19] Gunda, N. S. K., Singh, M., Norman, L., Kaur, K.., Mitra, S. K., “Optimization and characterization of biomolecule immobilization on silicon substrates using (3-aminopropyl)triethoxysilane (APTES) and glutaraldehyde linker,” Appl. Surf. Sci. **305**, 522–530 (2014).
[20] Schmidt, S., Flueckiger, J., Wu, W., Grist, S. M., Talebi Fard, S., Donzella, V., Khumwan, P., Thompson, E. R., Wang, Q., et al., “Improving the performance of silicon photonic rings, disks, and Bragg gratings for use in label-free biosensing,” SPIE Proc. **9166**(February), H. Mohseni, M. H. Agahi, and M. Razeghi, Eds., 91660M (2014).
[21] Vörös, J., “The density and refractive index of adsorbing protein layers.,” Biophys. J. **87**(1), 553–561, The Biophysical Society (2004).